Photon and neutrino-pair emission from circulating quantum ions

M. Yoshimura[1] and N. Sasao[2]

[1]*Center of Quantum Universe, Faculty of Science, Okayama University,
Tsushima-naka 3-1-1 Kita-ku, Okayama 700-8530, Japan*
[2]*Research Core for Extreme Quantum World, Okayama University,
Tsushima-naka 3-1-1 Kita-ku, Okayama 700-8530, Japan*

(Received 27 January 2016; published 29 June 2016)

The recent proposal of a photon and a neutrino-pair beam is investigated in detail. Production rates, both differential and total, of a single photon, two photons, and a neutrino pair emitted from quantum ions in circular motion are given for any velocity of ion. This part is an extension of our previous calculations at highest energies to lower energies of circulating ions, and hopefully helps to identify the new process of quantum ion circulation at a low energy ring. We clarify how to utilize the circulating ion for a new source of coherent neutrino beam despite much stronger background photons. Once one verifies that the coherence is maintained in the initial phases of time evolution after laser irradiation, large background photon emission rates are not an obstacle against utilizing the extracted neutrino-pair beam.

I. INTRODUCTION

Conventional sources of the neutrino beam have been decay products of elementary particles, pions for accelerator-based neutrino experiments, muons for atmospheric neutrino oscillation experiments, and unstable beta-nuclei for reactor-based neutrino experiments. It would be of great interest if one could add different kinds of neutrino beams having stronger flux and different features. Moreover, a related process, a gamma-ray beam with a large intensity (photons with energies larger than MeV), would be of interest in its own way and of great help to produce secondary intensive beams such as positron and neutron beams, which would provide other tools for future high energy physics experiments. A new mechanism of photon and neutrino-pair emission from circulating ions has recently been proposed [1] with these goals in mind.

The new mechanism of photon and neutrino-pair emission has some similarity to the synchrotron radiation [2–4], but also has important differences from the synchrotron radiation. The new proposal uses circulating quantum ions of mixed excited and ground states. When ions are circulated in the ground state, the formalism reduces to the usual synchrotron radiation: produced neutrinos and photons remain in the low energy region, typically in the keV range; hence one can essentially ignore the neutrino-pair emission due to extremely low production rates. But when quantum mixed states are circulated, it produces a completely different spectrum of more intensive fluxes in the high energy region, as demonstrated in our recent paper [1], which presented results in the high energy limit of ions. With the introduction of the quantum ion a new input of internal energy leads to a phase matching absent in the synchrotron radiation, providing large production rates of neutrino pairs and photons. Since ion deexcitation is

involved, produced neutrinos appear in the pair, $\nu_i \bar{\nu}_i$, $i = e, \mu, \tau$, which is quite unique to this beam. It would be ideal for *CP* violation oscillation experiments, since the beam itself is *CP*-even [5,6]. Application of a gamma-ray beam to a strong neutron source has also been worked out recently [7].

In the present work we shall deepen the understanding of the production mechanism of photons and neutrino pairs from a quantum ion ring and calculate basic quantities of production rates at any velocity of circular motion. This is expected to help verify experimentally important features of this new process.

The rest of this work is organized as follows. In Sec. II we recapitulate basic features of particle emission from a quantum ion beam and derive the fundamental differential rate for single-photon emission at any ion velocity. At the end of this section we discuss decoherence of a quantum ion beam during its circulation. In Sec. III outputs of analytical and numerical results are presented for the photon energy spectrum near the forward direction and the angular distribution, paying special attention to how these are changed with ion circulation velocity or the boost factor. Section IV discusses the neutrino-pair emission and how circulating heavy ions may become a strong source of the neutrino-pair beam, regardless of even stronger backgrounds of photon emission. In Appendix A we discuss the two-photon emission. In Appendix B we give some relevant mathematical items related to the subject in the present work. The mechanism of amplified emission discussed in the text is shown to be related to the parametric amplification that occurs in the Floquet system of differential equations having periodic coefficients.

Throughout this work we use the natural units of $\hbar = c = 1$.

II. PHOTON EMISSION FROM QUANTUM ION BEAM: BASIC FEATURES

We shall extend derivation of fundamental formulas of the photon emission rate of [1] to include cases of low velocity (small $\beta = v/c$) regions.

The quantum coherent state of a single ion (in the Schrödinger picture) is defined by a superposition of two states, $|e\rangle$ and $|g\rangle$,

$$|c(t)\rangle = \cos\frac{\theta_c}{2} e^{-i\epsilon_g t/\gamma}|g\rangle + \sin\frac{\theta_c}{2} e^{-i\epsilon_e t/\gamma}e^{i\varphi_c}|e\rangle. \quad (1)$$

We assume $|e\rangle$ to be a metastable excited state, while $|g\rangle$ is the ground state of the ion. The state $|c(t)\rangle$ is not an energy eigenstate unless $\theta_c/2 = 0$, $\pi/2$, but may be realized after laser irradiation. Without a loss of generality we may take $\varphi_c = 0$, which we shall do in the following. The boost factor $\gamma = 1/\sqrt{1-\beta^2}$, with β the velocity of a circulating ion divided by the light velocity.

The coherent state given by Eq. (1) is prepared *in situ*, most likely in a straight section just upstream of an extraction part, by laser irradiation from a counterpropagating direction. The actual choice of laser system, such as the number of lasers, their wavelengths, and intensities, depends upon the properties of the ions in use, in particular the energy gap ϵ_{eg} between $|e\rangle$ and $|g\rangle$, and their mutual parity. For example, in the most simple case of $|e\rangle$ being accessible from $|g\rangle$ by the electric dipole transition (E1), the $\pi/2$-pulse method [8], a well-established method in atomic physics experiments, may be employed with the wavelength corresponding to ϵ_{eg}/γ, taking into account the boost factor felt by the ions. Notice that the counterpropagating direction is chosen so that the maximum available photon energy $2\gamma\epsilon_{eg}$ is as large as possible while keeping the laser's photon energy low enough.

We assume that a single ion in this quantum state is circulating in the ring of radius ρ such that its orbit is

$$\vec{r}_I(t) = \rho\left(\sin\frac{\beta t}{\rho}, \cos\frac{\beta t}{\rho} - 1, 0\right), \quad (2)$$

in a coordinate system of $\vec{r}_I(0) = 0$. ($\beta = v/c$ here and below is meant to be the velocity of circulating ions, with the natural unit of the light velocity $c = 1$.) We consider coherent emission of many photons of definite momentum,

$$\vec{k} = \omega(\cos\psi\cos\theta, \cos\psi\sin\theta, \sin\psi), \quad (3)$$

and some helicity from a circulating single ion.

We consider the photon emission by electric dipole (E1) interaction. Extension to the magnetic dipole (M1) transitions is straightforward. The probability amplitude of an E1 photon is given using an expectation value of $|c(t)\rangle$:

$$\mathcal{M}(t) = \int_0^t dt' \langle c(t')| \frac{e\vec{p}}{m_e} |c(t')\rangle \cdot \vec{A}(t'; \vec{k}, h) \quad (4)$$

$$= -i\frac{\epsilon_{eg}}{\sqrt{2\omega V}}\int_0^t dt' \langle c(t')|\vec{d}|c(t')\rangle \cdot \vec{e}_h e^{i\omega t' - i\vec{k}\cdot\vec{r}_I(t')}. \quad (5)$$

V is the quantization volume of emitted electromagnetic field. This is a coherent sum along the orbit trajectory of a single ion. The production rate is defined by the time derivative of the probability; hence it is given by

$$\partial_t |\mathcal{M}(t)|^2 = 2\Re\left(\langle c(t)|\frac{e\vec{p}}{m_e}|c(t)\rangle \cdot \vec{A}(t; \vec{k}, h)\mathcal{M}(t)^*\right). \quad (6)$$

It is important from the fundamental physics point of view to use the $p \cdot A/m$ gauge instead of the $d \cdot E$ gauge often used in atomic physics calculation. These two gauges give approximately identical results when photons are nearly on the mass shell, namely, $\omega \sim \epsilon_{eg}$, but they may give completely different answers when photons are far off the mass shell, namely, $\omega \gg \epsilon_{eg}$ in our problem. We typically deal with cases of $\omega/\epsilon_{eg} = O(\gamma)$, which may be very large. Differences of rates in dependences on the boost factor γ are large in the two gauges.

Consider a situation in which all emitted photons of definite momentum $\vec{k}$ are collected by some detector. We sum over all available ions of the number $I 2\pi\rho/Q$, where I is the DC current of a heavy ion of charge Q. The total emission rate from all ion sources is

$$d\Gamma = \frac{Vd^3k}{(2\pi)^3}\frac{2\pi\rho I}{Q}\gamma\sum_h 2\Re\left(\langle c(t)|\frac{e\vec{p}}{m_e}|c(t)\rangle \cdot \vec{A}(t; \vec{k}, h)\mathcal{M}(t)^*\right), \quad (7)$$

$$2V\Re\left(\langle c(t)|\frac{e\vec{p}}{m_e}|c(t)\rangle \cdot \vec{A}(t; \vec{k}, h)\mathcal{M}(t)^*\right)$$

$$= \frac{\epsilon_{eg}^2}{\omega}(\sin\theta_c\cos\theta_c)^2\sum_{pol}e_h^i(e_h^j)^*(d_{eg})_i(d_{eg})_j\cos\tilde{\Phi}(0)$$

$$\times \int_0^t dt'\cos\tilde{\Phi}(t'), \quad (8)$$

$$\tilde{\Phi}(t) = \left(\omega - \frac{\epsilon_{eg}}{\gamma}\right)t - \rho\omega\cos\psi\left(\sin\left(\theta + \frac{\beta t}{\rho}\right) - \sin\theta\right). \quad (9)$$

The need to insert the boost factor γ is explained in [1].

Note that the emission rate from the excited state $|e\rangle$ does not have this type of time integral, since the factor ϵ_{eg}/γ is missing in Eq. (9) in that case. It leads to the usual synchrotron radiation [2] from the state $|e\rangle$, and the

emitted photons have much lower energies than of order 1 keV (and much smaller rates in the neutrino-pair emission). The reason for this behavior is due to the positive definiteness of the phase factor $\tilde{\Phi}(t)$ in the case without the $-\epsilon_{\text{eg}}/\gamma$ term, which leads to an exponential damping as ω increases. On the other hand, emission from the quantum state $|c(t)\rangle$ has the extra contribution in the phase $\tilde{\Phi}(t)$ from the internal ion energy $\propto \epsilon_{\text{eg}}$, which competes with the orbital contribution, giving rise to a kind of nonlinear resonance at the stationary phase points of $\partial_t \tilde{\Phi}(t) = 0$.

It is convenient for a comparison to introduce new angle variables tangential to the circulating ion:

$$(\theta', \psi') = (\theta + u, \psi), \tag{10}$$

such that $\theta' = 0$ corresponds to the tangential direction at different time $t = u\rho/\beta$. The phase integral multiplied by the photon momentum phase space is then

$$d\Omega \int_0^u dy \cos \Phi(y; \theta', \psi) = \int_0^u dy d\Omega' \cos \Phi(y; \theta', \psi). \tag{11}$$

Keeping in mind a photon extraction scheme in the outside of the ring, one may take small angular regions $\propto \Delta\theta$ near the tangential direction of $\theta' = 0$,

$$d\Omega' = \Delta\theta d\psi \cos \psi,$$

$$d\Omega \int_0^u dy \cos \Phi(y; \theta' = 0, \psi)$$

$$\sim \Delta\theta d\psi \cos \psi \int_0^u dy \cos \Phi(y; 0, \psi). \tag{12}$$

Written in terms of the new angular variable θ', we compare two terms in Eq. (9) ($u = \beta t/\rho$),

$$\sin(\theta + u) - \sin\theta = \sin\theta' + \sin(u - \theta')$$
$$= (1 - \cos u) \sin\theta' + \sin u \cos\theta'. \tag{13}$$

Near the tangential direction of $\theta' = 0$, the first term in the last equality of Eq. (13) is small, both because of $\theta' \sim 0$ and a small phase u region contributing to the large rate. In order to verify this assertion, we numerically simulated the phase integral, keeping fixed the tangential angle θ' at finite, nonvanishing values in Eq. (13). The result is illustrated in Fig. 1. Simulations suggest that the phase integrals for tangential angular regions of small, but finite $|\theta'| < 0.1$ (solid and dotted black curves in Fig. 1) agree well in $u < O(0.1)$. Moreover, the agreement in the time phase region of nearly all 2π range except at points close to 2π is good for smaller angle
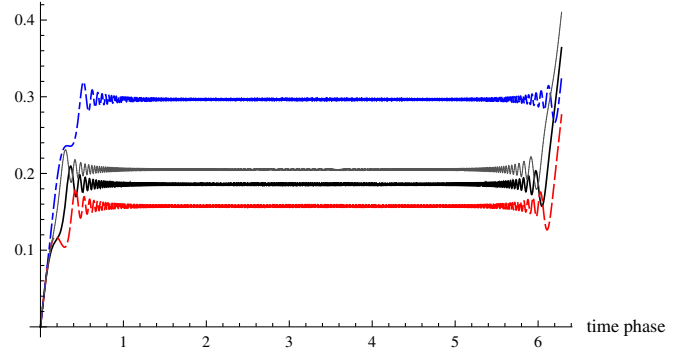

FIG. 1. Nonforward phase integral $\int_0^u dy \cos \Phi(y; \theta')$ for a few values of θ': 0.05 in solid black, 0.1 in dashed red, 0.2 in dotted-dashed blue, and 0 in dotted black. A two-period ion circulation of $u = 0 \sim 4\pi$ was taken for the end point of the time integral without decoherence. Assumed parameters are $b = 10^3$, $a = 1.01b$.

regions of $< O(0.05)$. This phase region includes the most important initial phases (regions up around $\pi/4$), smoothly matching to the stable plateau of large phase integral. It would be interesting to understand more deeply these behaviors from the point of the Floquet system described in Appendix B.

In most of the following discussions we shall suppress the angular θ' dependence by fixing it at zero. Thus, we shall use

$$\Phi(u; a, b) = bu - a \sin u,$$
$$a = \rho\omega \cos\psi,$$
$$b = \frac{\rho}{\beta}\left(\omega - \frac{\epsilon_{\text{eg}}}{\gamma}\right), \tag{14}$$

$$\int_0^t dt' \cos \tilde{\Phi}(t') = \frac{\rho}{\beta} \int_0^{\beta t/\rho} du \cos \Phi(u; a, b). \tag{15}$$

Taking summation over photon polarization (helicity) gives the differential spectrum of the form,

$$\frac{d^2\Gamma}{d\omega d\Omega} = \frac{2}{3(2\pi)^2} N d_{\text{eg}}^2 \epsilon_{\text{eg}}^2 \omega\gamma \frac{\rho}{\beta} \int_0^{\beta t/\rho} du \cos \Phi(u),$$
$$N = |\rho_{\text{eg}}(t)|^2 \frac{\rho I}{Q}, \tag{16}$$

with $|\rho_{\text{eg}}(t)| = \sin \theta_c/2$. N is the number of coherent ions available for photon emission in the beam.

The radius ρ of circular ion motion is of macroscopic length, and one may take the infinite radius limit in the sense $\rho\epsilon_{\text{eg}} \gg 1$. The largest contribution to the rates in the large radius limit arises from the large region of a, b in the phase function $\Phi(u)$. The numerical result for the ion level spacing of 5 eV gives

$$\rho\epsilon_{eg} = 2.5 \times 10^{10} \frac{\rho}{1 \text{ km}} \frac{\epsilon_{eg}}{5 \text{ eV}}. \tag{17}$$

We consider the detection of emitted photons after irradiating lasers from counterpropagating directions. The counterpropagating direction is chosen both to create a high coherence and to utilize laser frequencies boosted by the factor 2γ for the best match to a deeper level spacing of ions. Detectors are usually placed in a transport system tangential to the ion circular motion. The transport system for the photon extraction has a finite angular coverage $\Delta\theta$ in the ion beam plane, and one should consider emitted photons from circulating ions in a limited time interval Δt, which is related to the detected angular aperture $\Delta\theta$ by $\Delta t = \rho r \Delta\theta/v$, r being of order the ratio of the distance to the detector to the circular radius to R/ρ. The question now arises on where the extraction system is to be placed in relation to the laser irradiation point.

It is shown in Appendix B that the Bessel function is relevant to the emission rate at one-period revolution $u = 2\pi$ of ion motion after laser irradiation. It is however necessary to calculate emission rates at any phase angle u prior to one period of circulation. Consider for this purpose the phase integral,

$$\int_0^u du' \cos(bu' - a\sin u'). \tag{18}$$

We are unaware of any simple analytic function that gives this integral accurately. Extensive numerical studies of this function for large a, b's have been done accordingly. A typical result is shown in Fig. 4 along with a truncated approximation to the third order in u of the phase function. There is a wide region of the phase u giving a nearly flat plateau of integral value at the half of the full integral, which is $\pi J_b(a)$ (the Bessel function of order b and argument a). For the parameter range $a \gg a - b > 0$, $\pi J_b(a) \sim \sqrt{\pi}(a^2 - b^2)^{-1/4}$. See the Appendix for more details. A stable photon emission rate is expected in this plateau region, which is excellent for the purpose of extracting a large flux of photons as a beam. The initial behavior of emission rate at $u \ll 1$ shall be discussed in Sec. IV.

The differential spectrum rate in the stable extraction region is then given, using a dimensionless energy $x = \omega/\epsilon_{eg}$, by

$$\frac{d^2\Gamma}{dxd\Omega} = \frac{A_{eg}}{2\sqrt{\pi}} N \sqrt{\frac{\rho\epsilon_{eg}}{\beta}} \gamma x \left(\beta^2 x^2 \cos^2\psi \cos^2\theta \right.$$
$$\left. - \left(x - \sqrt{1-\beta^2}\right)^2\right)^{-1/4}, \tag{19}$$

$$x_- \leq x \leq x_+, \qquad x_\pm = \sqrt{\frac{1 \pm \beta}{1 \mp \beta}}, \tag{20}$$

with the Einstein coefficient (decay rate) given by $A_{eg} = d_{eg}^2\epsilon_{eg}^3/3\pi$. This is our fundamental formula giving the angular distribution and the energy spectrum of photon emission. The overall rate factor is numerically given by

$$\frac{1}{2\sqrt{\pi}} A_{eg} N \sqrt{\rho\epsilon_{eg}} = 2.82 \times 10^{15} \text{ Hz} \frac{A_{eg}}{1 \text{ kHz}} \sqrt{\frac{\rho\epsilon_{eg}}{10^{10}}} \frac{N}{10^8}. \tag{21}$$

It is important to clarify how the coherence $\rho_{eg}(t)$ changes during ion circulation. In the formulas above we defined the effective number of ions as the circulating number of ions times the coherence squared $|\rho_{eg}|^2$. This coherence decays with the emission of photons of rates proportional to $|\rho_{eg}(t)|^2$. The basic equation of the time dependence and its solutions for the coherence loss are thus

$$\frac{d\rho_{eg}}{dt} = -\frac{K}{2}\rho_{eg}^3,$$

$$\rho_{eg}(t) = \frac{\rho_{eg}(0)}{\sqrt{1 + K\rho_{eg}^2(0)t}},$$

$$\rho_{eg}(0) = \frac{1}{2}\sin(\theta_c), \tag{22}$$

$$K = \frac{A_{eg}}{\sqrt{\pi}} \sqrt{\rho\epsilon_{eg}} \frac{\pi}{\gamma\sqrt{\beta}} \int dx x \left(\beta^2 x^2 - \left(x - \frac{1}{\gamma}\right)^2\right)^{-1/4}, \tag{23}$$

where K was calculated by integrating the photon number over all emitted photon energies x ($\sqrt{\frac{1-\beta}{1+\beta}} \leq x \leq \sqrt{\frac{1+\beta}{1-\beta}}$ reduced in the high energy limit to $0 < x < 2\gamma$ in the dimensionless energy units used here) and angular area π/γ^2. It is interesting to note that the asymptotic value in $t \gg 1/(K\rho_{eg}^2(0))$ is independent of the initial coherence $\rho_{eg}(0)$, $\rho_{eg}(t) \to 1/\sqrt{Kt}$. We assumed the reality of the coherence, since the phase factor is not important.

It is assumed in this discussion of decoherence that there exists no other important relaxation process. This assumption is reasonable when the laser is irradiated after ions reach their highest energy in the ring and the number of circulating ions is scarce with negligible mutual interaction.

The actual amount of decoherence is dependent on details of the acceleration scheme, in particular where the extraction of the beam is made after the point of laser irradiation. For simplicity we shall extract photon or neutrino-pair beams right after the laser irradiation; hence we ignore the decoherence effect, keeping in mind that the degree of decoherence is in principle calculable.

III. ENERGY SPECTRUM IN THE FORWARD DIRECTION AND ANGULAR DISTRIBUTION

In this section basic quantities relevant to the detection of extracted photons are calculated in the stable plateau region of phases $< O(\pi/4)$. Outside this region the approximation that neglects the term $1 - \cos u$ in Eq. (13) is questionable. We first show the photon energy spectrum in the forward direction. For this purpose we integrate the fundamental formula, Eq. (19), over a small solid angle area $\pi\Delta^2$ in the forward direction $\psi = \theta = 0$. This can be done using

$$\int_{\sqrt{\psi^2+\theta^2}\leq\Delta} d\psi\, d\theta (A^2 - B^2(\psi^2 + \theta^2))^{-1/4}$$
$$= \frac{4\pi}{3}\frac{1}{B^2}(A^{3/2} - (A^2 - B^2\Delta^2)^{3/4}). \quad (24)$$

Taking A^2, B^2 relevant to our problem and expanding in terms of the small angle factor Δ^2, one finds that

$$\int_{\sqrt{\psi^2+\theta^2}\leq\Delta} d\psi\, d\theta \left(\beta^2 x^2\cos^2\psi\cos^2\theta - \left(x - \sqrt{1-\beta^2}\right)^2\right)^{-1/4}$$
$$\sim \pi\Delta^2\gamma^{1/2}((x - x_-)(x_+ - x))^{-1/4}, \quad (25)$$

in the limit $\gamma \to \infty$. This formula is valid in a limited region of Δ^2, which gives a Δ-dependent range of allowed photon energies:

$$\frac{1}{1+\beta^2\gamma^2\Delta^2}\left(\gamma - \sqrt{\gamma^2(1-\beta^2\Delta^2) - 1}\right)$$
$$\leq x \leq \frac{1}{1+\beta^2\gamma^2\Delta^2}\left(\gamma + \sqrt{\gamma^2(1-\beta^2\Delta^2) - 1}\right). \quad (26)$$

The forward energy spectrum rate is given by either of the following two forms,

$$\left(\frac{d\Gamma}{dx}\right)_0 = N\pi\Delta^2\frac{A_{eg}}{2\sqrt{\pi}}\sqrt{\rho\epsilon_{eg}}\frac{\gamma^{3/2}}{\sqrt{\beta}}x((x-x_-)(x_+ - x))^{-1/4},$$
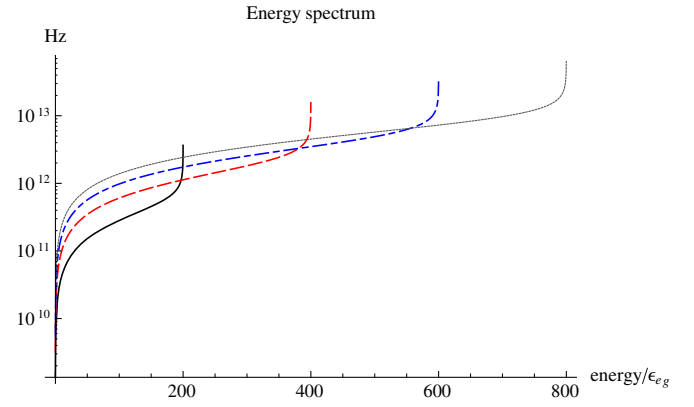$$\quad (27)$$

FIG. 2. Photon energy spectrum per unit solid angle area [Eq. (27) divided by $\pi\Delta^2$] at the forward direction for a few choices of the boost factor: $\gamma = 100$ in solid black, 200 in dashed red, 300 in dash-dotted blue, and 400 in dotted black. The angular resolution of $\Delta = 0.01/\gamma$ was taken here. Other assumed parameters are $A_{eg} = 1$ kHz, $\rho\epsilon_{eg} = 10^{10}$, $N = 10^8$ and rates scale as $\propto A_{eg}\sqrt{\rho\epsilon_{eg}}N$.

$$\left(\frac{d\Gamma}{dy}\right)_0 \to N\pi\Delta^2\frac{A_{eg}}{\sqrt{2\pi}}\sqrt{\rho\epsilon_{eg}}\gamma^2 y^{3/4}(1-y)^{-1/4},$$
$$y = \frac{\omega}{\omega_{max}} \sim \frac{\omega}{2\gamma\epsilon_{eg}}, \quad \text{as } \gamma \to \infty. \quad (28)$$

We expect under normal experimental circumstances that $\Delta \leq O(1/\gamma)$. In Fig. 2 we illustrate the forward energy spectrum per unit solid angle area $\pi\Delta^2 = 1$. The Jacobian peak at the highest energy is clearly visible for smaller values of the angular resolution Δ, which degrades when the angular coverage Δ becomes larger, for instance, at $\Delta \geq O(0.1)/\gamma$. The Jacobian peak suggests a high degree of a correlation between the photon energy and its emission angle.

We next calculate the angular distribution after the photon energy integration. The formula of angular integration gives

$$\frac{d\Gamma}{d\Omega} = \frac{1}{2\sqrt{\pi}}NA_{eg}\sqrt{\rho\epsilon_{eg}}\frac{\gamma}{\sqrt{\beta}}\int_{X_-}^{X_+} dx \frac{x}{\left(\beta^2 x^2\cos^2\psi\cos^2\theta - \left(x - \sqrt{1-\beta^2}\right)^2\right)^{1/4}} \quad (29)$$

$$= c_0 NA_{eg}\sqrt{\rho\epsilon_{eg}}\gamma^{-1/2}\frac{\sqrt{\cos\psi\cos\theta}}{(1-\beta^2\cos^2\psi\cos^2\theta)^{7/4}} \to c_0 NA_{eg}\sqrt{\rho\epsilon_{eg}}\gamma^3\frac{1}{(1-\gamma^2(\psi^2+\theta^2))^{7/4}}, \quad (30)$$

$$X_\pm = \frac{1}{\gamma(1\mp\beta\cos\psi\cos\theta)}, \qquad c_0 = 2\frac{\Gamma(\frac{3}{4})}{\Gamma(\frac{1}{4})} = 0.676. \quad (31)$$

This angular distribution is illustrated in Fig. 3. The forward peaking as the boost factor increases is clearly observed already at intermediate γ values.
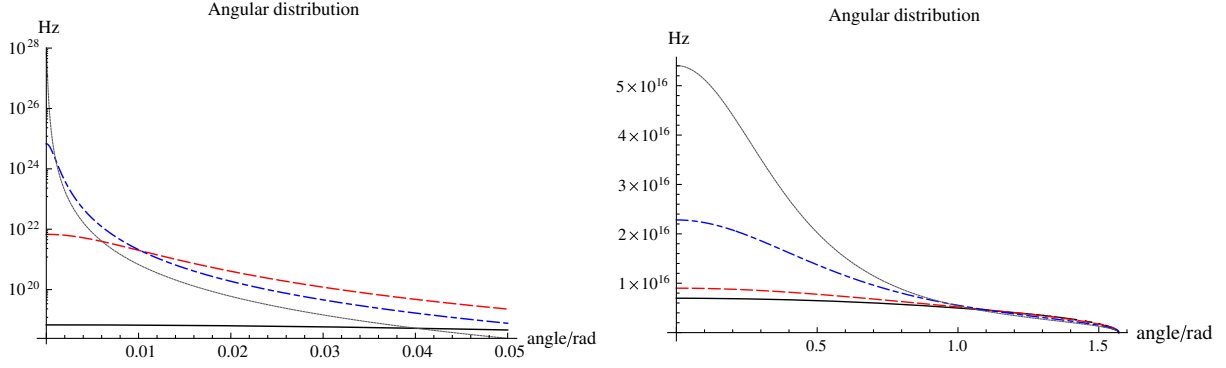
FIG. 3. Angular distribution either at $\psi = 0$ or $\theta = 0$ in the single-photon emission for a few choices of the boost factor. In the left panel $\gamma = 10$ in solid black, 100 in dashed red, 1000 in dotted-dashed blue, and 10^4 in dotted black. In the right panel $\gamma = 1.01$ in solid black, 1.1 in dashed red, 1.5 in dotted-dashed blue, and 2 in dotted black. Other assumed parameters are $A_{eg} = 1$ kHz, $\rho\epsilon_{eg} = 10^{10}$, $N = 10^8$ and rates scale as $\propto A_{eg}\sqrt{\rho\epsilon_{eg}}N$.

Finally, we calculate the total photon emission rate by integrating both energy and angle variables. The result is given by

$$\Gamma \sim 2.8NA_{eg}\sqrt{\rho\epsilon_{eg}}\gamma, \tag{32}$$

which holds in both large γ and small β limits.

We observe that compared to the spontaneous emission rate $A_{eg}N$, the quantum ion beam gives rise to a rate enhanced by a factor $\propto \sqrt{\rho\epsilon_{eg}}$, except the factor $\propto \gamma$. Since ρ is of a macroscopic size and is much larger than the microscopic scale $1/\epsilon_{eg}$, this may become gigantic.

A nontrivial aspect of γ-dependence should be noted for the collimated photon emission. For a large γ the angular coverage is very much limited to an angular area of order $1/\gamma^2$ and the total rate is diminished by this coverage factor. This means that in a unit solid angle area in the forward narrow cone the differential angular rate is effectively of the order γ^2 larger than the total rate.

Calculations so far presented are exact except the use of an approximate form of the large order Bessel function. An alternative method of total rate calculation is to treat the angular variables θ, ψ symmetrically, and to approximate the product function

$$\cos^2\psi\cos^2\theta \sim 1 - (\psi^2 + \theta^2), \tag{33}$$

which is valid at large γ's, showing the highly collimated angular distribution. This method can readily be extended to the case of multiple particle emission such as the neutrino-pair emission. To make the behavior of the rates in the high energy limit ($\gamma \to \infty$) more transparent, it is convenient to use the energy rescaled by the maximum energy $x_+\epsilon_{eg}$ and to introduce the variable y defined below. Resulting rates are as follows:

$$\frac{d\Gamma'}{dy} = c_3A_{eg}N\sqrt{\rho\epsilon_{eg}}G(y), \qquad c_3 = \frac{4\sqrt{2\pi}}{3} = 3.34,$$

$$y = \frac{x}{x_+}, \qquad y_- \leq y \leq 1, \qquad y_- = \frac{1-\beta}{1+\beta}, \tag{34}$$

$$G(y) = \frac{((y-y_-)(1-y))^{3/4}}{y}. \tag{35}$$

A more useful approximation to treat the total rate at any velocity is given by

$$\Gamma' = c_4A_{eg}N\sqrt{\rho\epsilon_{eg}}\gamma, \qquad c_4 = \frac{4\sqrt{2\pi}}{3}B\left(\frac{3}{4},\frac{7}{4}\right) = 2.83. \tag{36}$$

The agreement of the parameter dependence and an excellent closeness of constants in Eqs. (32) and (36) gives confidence in the approximation here.

One may use a truncated time expansion in the initial and intermediate phase region for an estimate of the crucial phase integral. We thus expand the phase function $\Phi(u)$ in terms of the circulating phase variable u to its third order:

$$\Phi(u) \sim -(a - b)u + \frac{a}{6}u^3. \tag{37}$$

This approximation is compared with the exact phase integral in Fig. 4. It is thus clear that the third order approximation is excellent except in a small region near the returning phase point of $u = 2\pi$.

For further analytic calculations it is important to locate stationary points of the phase integral. The stationary phase point given by the vanishing derivative $\Phi'(u) = 0$ exists at

$$u = u_\pm = \pm\sqrt{\frac{2(a-b)}{a}}, \qquad \text{for } \frac{a-b}{a} \geq 0. \tag{38}$$
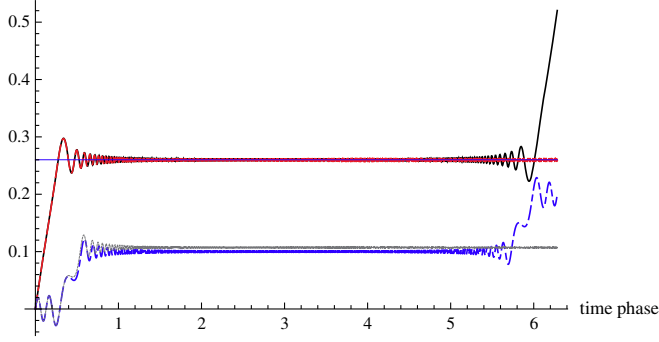
Phase integral and its approximation

FIG. 4. Approximate phase integral by truncation to the third order compared with exact results: exact case of $(b, a) = 500(1, 1.01)$ in solid black, its approximate case in dashed red, exact case of $(b, a) = 500(1, 1.1)$ in dotted-dashed blue, and its approximate case in dotted black. The straight line shows the $J_b(a)$ value for $(b, a) = 500(1, 1.01)$.

The Gaussian phase approximation to this function and the resulting phase integral give

$$\Phi(u) \sim -\frac{2\sqrt{2}}{3}(a - b)\sqrt{\frac{a - b}{a}}$$
$$+ \sqrt{\frac{a(a - b)}{2}}\left(u - \sqrt{\frac{2(a - b)}{a}}\right)^2, \quad (39)$$

$$\int_0^u dy \cos \Phi(y) \sim \left(\frac{2}{a(a - b)}\right)^{1/4}$$
$$\times \Re\left(e^{-iX}\int_0^Y dz \exp[i(z - W)^2]\right), \quad (40)$$

$$X = \frac{2\sqrt{2}}{3}(a - b)\sqrt{\frac{a - b}{a}},$$
$$Y = u\left(\frac{a(a - b)}{2}\right)^{1/4},$$
$$W = b\left(\frac{2}{a(a - b)}\right)^{1/4}. \quad (41)$$

In the limit of $Y \gg W$, one may replace $Y \to \infty$, $W \to 0$ to derive a Fresnel type of integral in an infinite range,

$$\int_0^\infty dy \cos \Phi(y) \sim \left(\frac{2}{a(a - b)}\right)^{1/4}\frac{\sqrt{\pi}}{2}\cos\left(X - \frac{\pi}{4}\right). \quad (42)$$

Inserting relevant quantities for a, b gives

$$\frac{d^2\Gamma}{dxd\Omega} = \frac{1}{2^{9/2}\sqrt{\pi}}A_{eg}N\sqrt{\rho\epsilon_{eg}}\frac{(1 + \beta)^{1/4}}{\beta^{3/4}}\gamma^{3/2}F_{1g}(x), \quad (43)$$

$$F_{1g}(x) = x\left(x(x_+ - x) - \frac{\beta(1 + \beta)}{2}\gamma^2 x^2(\theta^2 + \phi^2)\right)^{-1/4}$$
$$\times \cos\left(\frac{\rho\epsilon_{eg}}{3}(\sqrt{\beta(1 + \beta)}\gamma)^{-3}x\right.$$
$$\times \left.\left(\frac{x_+ - x}{x} - \frac{\beta(1 + \beta)}{2}\gamma^2(\theta^2 + \phi^2)\right)^{3/2} - \frac{\pi}{4}\right). \quad (44)$$

The major difference from the previous formula (19), in particular at large γ's, is the presence of the oscillating function having an interesting combination of large factors, $\rho\epsilon_{eg}/\gamma^2$ with $x \propto \gamma$; all other factors are in reasonable agreement with the previous result. Another difference is the low β behavior, arising from $\propto (a(a - b))^{-1/4}$, which should be compared with the previous approximation from the Bessel function giving $\propto (a^2 - b^2)^{-1/4}$. Although the difference at large γ's is minor, the low β behavior is quite different. Indeed, the stationary phase approximation here cannot reproduce the correct behavior $\propto \sqrt{\beta}$ in the total rate.

The formula (43) is valid for the time or its related phase domain,

$$t > t_*,$$

$$t_* = \rho\sqrt{\frac{2}{\beta(1 + \beta)}}\frac{1}{\beta\gamma}\left(\frac{x_+ - x}{x} - \frac{\beta(1 + \beta)}{2}\gamma^2(\theta^2 + \psi^2)\right)^{1/2}. \quad (45)$$

Due to the oscillating factor the major contribution arises from the photon phase space region of
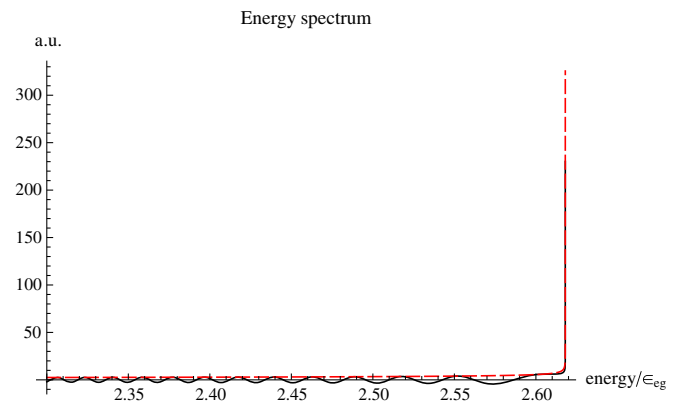
Energy spectrum

FIG. 5. Effect of oscillatory behavior in the forward energy spectrum. Formula given by Eq. (44) with (solid black) and without (dashed red) the sinusoidal function. Assumed parameters are the $\gamma = 1.5$, $\rho\epsilon_{eg} = 10^{14}$ case in dotted black.

$$\frac{x}{x_+}\left(\frac{x_+ - x}{x} - \frac{\beta(1+\beta)}{2}\gamma^2(\theta^2 + \psi^2)\right)^{3/2}$$
$$< \frac{3}{\rho\epsilon_{eg}}\beta^{3/2}(1+\beta)^{1/2}\gamma^2. \tag{46}$$

The combination of parameters that appear here is of order,

$$\frac{\gamma^2}{\rho\epsilon_{eg}} = 10^{-4}\left(\frac{\gamma}{10^3}\right)^2\frac{10^{10}}{\rho\epsilon_{eg}}. \tag{47}$$

At the quantitative level the effect of the oscillatory term is important only at low γ's. We illustrate an example in Fig. 5, which shows that the oscillation effect is not significant at energies contributing to large rates.

IV. NEUTRINO-PAIR EMISSION RATES

The cases of multiple particle emission, in particular a neutrino pair, are of great interest. Our formalism may be directly extended to these cases, which we shall turn to.

For simplicity we shall take massless neutrinos of three flavors, which is an excellent approximation for neutrino energies E_i much larger than their masses. Quantities that appear in the phase integral are changed to

$$\Phi(u) = bu - a\sin u,$$
$$b = \frac{\rho}{\beta}\left(E_1 + E_2 - \frac{\epsilon_{eg}}{\gamma}\right),$$
$$a = \rho(E_1\cos\psi_1\cos\theta_1 + E_2\cos\psi_2\cos\theta_2). \tag{48}$$

Matrix element factors are readily worked out by squaring the electron spin transition moment $\vec{S}_e = \langle g|\vec{\sigma}|e\rangle/2$ arising from the axial vector part of the four-Fermi interaction as in [1]. The calculated differential rate for three neutrino flavor pairs is

$$\frac{d^4\Gamma_{2\nu}}{dy_1 dy_2 d\Omega_1 d\Omega_2} = \frac{\sqrt{\pi}}{16(2\pi)^6}G_F^2\epsilon_{eg}^5 N\sqrt{\rho\epsilon_{eg}}\vec{S}_e^2\left(1 + \frac{2}{3}\beta^2\gamma^2\right)\frac{1}{\sqrt{\beta}\gamma}x_+^6$$
$$\times y_1^2 y_2^2\left(1 + \frac{1}{3}\cos\psi_1\cos\psi_2\cos(\theta_1 - \theta_2) + \frac{1}{3}\sin\psi_1\sin\psi_2\right)$$
$$\times\left(\beta^2(y_1\cos\psi_1\cos\theta_1 + y_2\cos\psi_2\cos\theta_2)^2 - \left(y_1 + y_2 - \frac{1}{\gamma x_+}\right)^2\right)^{-1/4}, \tag{49}$$

with $x_+ = \sqrt{(1+\beta)/(1-\beta)} \sim 2\gamma$ and $y_i = E_i/(x_+\epsilon_{eg})$. After angular integrations that give the $O(\gamma^{-4})$ factor, one may derive a formula of the total pair emission rate,

$$\Gamma_{2\nu} = c_4 G_F^2\epsilon_{eg}^5 N\sqrt{\rho\epsilon_{eg}}\vec{S}_e^2\left(1 + \frac{2}{3}\beta^2\gamma^2\right)\beta^{-9/2}(1+\beta)^{11/2}\gamma I, \tag{50}$$

$$I = \int dy_1 dy_2\frac{y_1 y_2}{(y_1 + y_2)^2}((y_1 + y_2 - y_-)(1 - y_1 - y_2))^{7/4}, \tag{51}$$

$$c_4 = \frac{\sqrt{\pi}}{12(2\pi)^6}\int_{|\vec{x}|\leq 1}dv_4(1 - \vec{x}^2)^{-1/4}$$
$$= \frac{1}{128(2\pi)^3}\frac{\Gamma(3/4)}{\Gamma(13/4)} = 1.21 \times 10^{-4}, \tag{52}$$

$$c_4 G_F^2\epsilon_{eg}^5 N\sqrt{\rho\epsilon_{eg}} = 2.5\text{ Hz}\sqrt{\frac{\rho\epsilon_{eg}}{10^{14}}}\frac{N}{10^8}\left(\frac{\epsilon_{eg}}{10\text{ keV}}\right)^5. \tag{53}$$

The integral related to the constant c_4 is over the 4d volume of radius unity. For this estimate we took a large radius ρ of ion circular motion and the level spacing ϵ_{eg} appropriate for high energy neutrino-pair production.

Dependence of the total rate $\propto \gamma^3$ of Eq. (50) in the high energy limit is different from the $\propto \gamma^4$ in [1]. The difference is traced to a different angular distribution in the stationary phase approximation. In [1] the angular θ, ψ distribution is asymmetric, and it has a wider range of allowed angles in θ_i variables: only the relative opening angle $\theta_1 - \theta_2$ is limited by $1/\gamma$, but their individual θ_i's are not limited by this factor. This does not give an extra $1/\gamma$ suppression in the result of the total rate, which explains the difference from the present work. As to the total rate we believe that the present method is closer to the correct, more precise result. But it is important to note that what is to be compared with actual observations is the rate within a given aperture of angles, and this should be calculated more precisely by taking into account the geometry of the detector system. This way one may obtain an effective enhancement of a γ power.

In Fig. 6 we illustrate the forward spectrum rate of a single neutrino in the pair production process. The basic formula derived by taking $\psi_i = \theta_i = 0$ in Eq. (49) is given in terms of $y = x\sqrt{(1+\beta)/(1-\beta)}$,
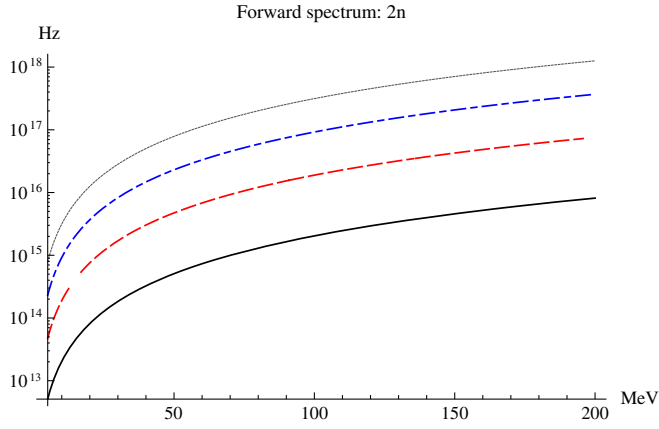
FIG. 6. Neutrino spectrum rate in the forward direction in neutrino-pair emission, assuming the overall factor of 0.05 Hz in Eq. (54). The chosen γ factors are 4000 in solid black, 6000 in dashed red, 8000 in dotted-dashed blue, and 10^4 in dotted black.

$$S(y) = 0.05 \text{ Hz} \sqrt{\frac{\rho\epsilon_{\text{eg}}}{10^{14}}} \frac{N}{10^8} \vec{S}_e^2 \left(1 + \frac{2}{3}\beta^2\gamma^2\right) \frac{(1+\beta)^6}{\sqrt{\beta}} \gamma^{11/2}$$

$$\times \int dy_2 y^2 y_2^2 ((y_1 + y_2 - y_-)(y_+ - y_1 - y_2))^{-1/4},$$

(54)

which is valid for rates per unit solid angle area in the forward direction of $\theta = \psi = 0$. The spin factor $\vec{S}_e^2 = 1$ and $N = 10^8$, $\rho\epsilon_{\text{eg}} = 10^{14}$ were taken for simplicity.

Now we would like to discuss a possible obstacle against detection of the neutrino-pair emission. Gigantic backgrounds of QED processes are not really a problem, because all emitted photons are beam-dumped by some experimental facility before the extracted neutrino-pair beam is used for experiments. The important question is whether the absolute neutrino-pair emission is large enough for experiments away from the ion ring. Our

calculations here show that when the circulating ion and the accelerator parameter are appropriately chosen, this is not a problem.

In summary, we presented both the differential and the total rates of produced single photons and neutrino pairs emitted from quantum ions in circular motion. When ions are in a quantum mixed state, the produced energy spectrum is completely different from the case of synchrotron radiation from circulating ions, opening a new method of unique production of a coherent neutrino-pair beam. Results were given for any velocity of circulating ion and hence should be useful for experimental investigations of these processes, for instance, pilot experiments of low energy photon emission. An important parameter region of energy and direction of emitted photons or neutrino pairs was derived by identifying where rate amplification occurs in the important time integral of the phase factor. In a sequel to the present work [6] we shall discuss how neutrino oscillation experiments can measure important parameters of neutrino properties.

APPENDIX A: RATES OF TWO-PHOTON EMISSION

Here we calculate rates of two-photon emission and discuss which of the single- or the two-photon emission is dominant for large boost values relevant to the large rate region of the neutrino-pair emission.

The differential spectrum of two-photon emission is calculated as

$$\frac{d^4\Gamma_{2\gamma}}{dy_1 dy_2 d\Omega_1 d\Omega_2} = \frac{\sqrt{\pi}}{4(2\pi)^4} N \frac{A_{pe}A_{pg}\epsilon_{\text{eg}}}{\epsilon_{pe}\epsilon_{pg}} \epsilon_{\text{eg}} \sqrt{\frac{\rho\epsilon_{\text{eg}}}{\beta}} (1+\beta)^6 \gamma^4 y_1 y_2 M(y_1, y_2)$$

$$\times \left(\beta^2\gamma^2(y_1\cos\psi_1\cos\theta_1 + y_2\cos\psi_2\cos\theta_2)^2 - \left(\gamma(y_1 + y_2) - \frac{1}{x_+}\right)^2\right)^{-1/4}, \quad (A1)$$

$$M(y_1, y_2) = \frac{1}{(y_1 + \epsilon_{pe}/(x_+\epsilon_{\text{eg}}))^2} + \frac{1}{(y_2 + \epsilon_{pe}/(x_+\epsilon_{\text{eg}}))^2} + \frac{3}{4}\frac{1}{(y_1 + \epsilon_{pe}/(x_+\epsilon_{\text{eg}}))(y_2 + \epsilon_{pe}/(x_+\epsilon_{\text{eg}}))}, \quad (A2)$$

with $y_i = \omega_i/(x_+\epsilon_{\text{eg}})$. The function M is the squared sum of energy denominator factors in the second order of perturbation theory. In this estimate of matrix element M we replaced a factor $(\vec{k}_1 \cdot \vec{k}_2/\omega_1\omega_2)^2$ in the interference term by its average $1/2$, which is not precise, but it would serve for our crude estimate.

The angular integrations over those of two photons may be explicitly done, using the expansion like $\cos\theta_i \sim 1 - \theta_i^2/2$, which should be valid for large boosts. The result after angular integrations is

$$\int d\Omega_1 \int d\Omega_2 ((y_1 + y_2 - y_-)(1 - y_1 - y_2) - \beta^2 \gamma^2 (y_1 + y_2)(y_1(\psi_1^2 + \theta_1^2) + y_2(\psi_2^2 + \theta_2^2)))^{-1/4}$$

$$= \frac{128}{231} \pi^2 \frac{\Gamma(3/4)}{\Gamma(13/4)} (\beta\gamma)^{-4} \frac{((y_1 + y_2 - y_-)(1 - y_1 - y_2))^{7/4}}{y_1 y_2 (y_1 + y_2)^2}. \tag{A3}$$

The single-photon spectrum shape after the second photon energy is integrated out is given by

$$\frac{d\Gamma_{2\gamma}}{dy} = 3.6 \times 10^9 \text{ Hz} \frac{\text{keV}\epsilon_{eg}}{\epsilon_{pe}\epsilon_{pg}} \frac{A_{pe}A_{pg}}{(10 \text{ MHz})^2} \sqrt{\frac{\rho\epsilon_{eg}}{10^{10}}} \frac{N}{10^8} \frac{(1+\beta)^2}{\beta^{9/2}} F_{2\gamma}(y), \tag{A4}$$

$$F_{2\gamma}(y) = \int dy_2 \left(\frac{1}{y + y_2}\right)^2 ((y + y_2 - y_-)(1 - y - y_2))^{7/4} M(y, y_2), \qquad y_- = \frac{1 - \beta}{1 + \beta}, \tag{A5}$$

with $x_+ = \sqrt{(1 + \beta)/(1 - \beta)}$.

Numerical results of the energy spectrum of a single photon in the two-photon emission process are illustrated in Fig. 7 for some values of the boost factor. The end point of energy spectrum increases with γ accompanied by a rate increase. In the high energy limit of $\gamma \gg 1$ the total rate of two-photon emission obeys the scaling law $\propto \gamma^4$ [1]. The two-photon emission of E1 × E1 type is usually weaker than M1 type emission, although the M1 rate is much smaller than the E1 rate.

APPENDIX B: MATHEMATICAL SUPPLEMENTS

1. Bessel function of large orders for large arguments

In order to calculate the phase integral of a type as in Eq. (18), we note the integral representation of a Bessel function that holds for noninteger ν's [9]:
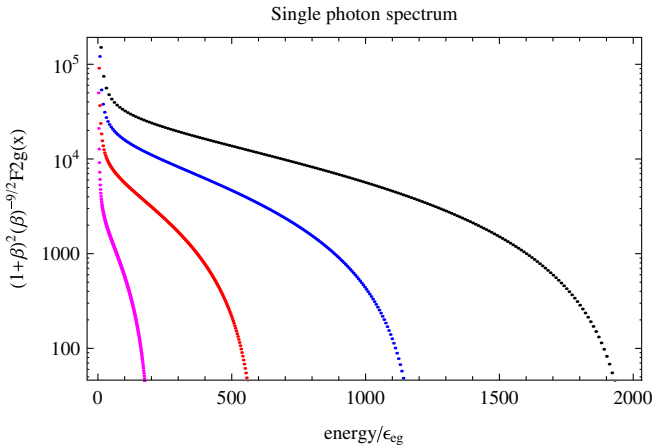
$$J_\nu(z) = \frac{1}{\pi} \int_0^\pi d\theta \cos(\nu\theta - z \sin\theta)$$
$$- \frac{\sin\nu\pi}{\pi} \int_0^\infty dt e^{-\nu t - z \sinh t}, \tag{B1}$$

which holds for $\Re\nu > 0$, $\Re z > 0$. The second integral is limited from above: for real and positive ν, z by

$$\left|\int_0^\infty dt e^{-\nu t - z \sinh t}\right| < \int_0^\infty dt e^{-(\nu + z)t} = \frac{1}{\nu + z}, \tag{B2}$$

which means that this second contribution is a small contribution in the large ν, z limit. We then work out the other half of the integration range,

$$\int_\pi^{2\pi} d\theta \cos(\nu\theta - z \sin\theta) = \Re\left(\int_0^\pi d\theta' e^{i\nu(\theta'-\pi) + z \sin\theta'}\right)$$
$$\sim \Re e^{-i\nu\pi} J_\nu(-z) = J_\nu(z). \tag{B3}$$

Thus, by neglecting the subleading terms,

$$J_\nu(z) = \frac{1}{2\pi} \int_0^{2\pi} d\theta \cos(\nu\theta - z \sin\theta) + O\left(\frac{1}{\nu + z}\right). \tag{B4}$$

The asymptotic behavior of the Bessel function,

$$J_\nu(\nu \sec\beta) = \sqrt{\frac{2}{\nu\pi \tan\beta}} \cos\left(\nu \tan\beta - \nu\beta - \frac{\pi}{4}\right), \tag{B5}$$

can be used to derive for $0 < a^2 - b^2 \ll |b| \to \infty$

$$J_b(a) \sim \frac{1}{\sqrt{\pi}} (a^2 - b^2)^{-1/4}. \tag{B6}$$

This limiting behavior is valid when $a^2 - b^2 \gg 1$. If $a^2 - b^2 = O(1)$, a function $f(1/(a^2 - b^2))$ which may be expressed in power series expansions multiplies. Since $a^2 - b^2 = O((\rho\epsilon_{eg})^2)$, the asymptotic form is usually

FIG. 7.   Energy spectrum shape of a single photon using $x = \omega/\epsilon_{eg}$ in two-photon emission for $\gamma = 100$ in magenta, 300 in red, 600 in blue, and 1000 in black. $\epsilon_{pe}/\epsilon_{eg} = 0.5$ is assumed.
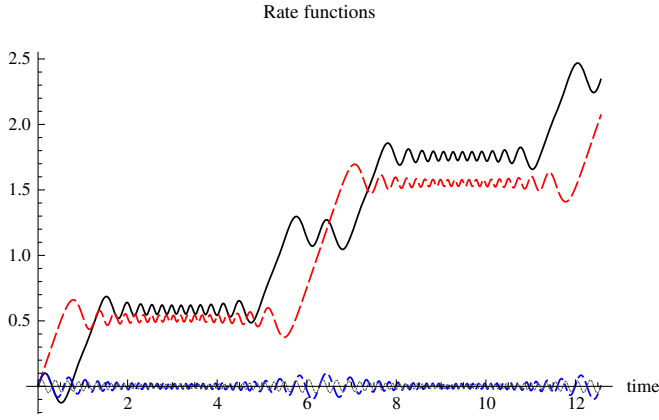
Rate functions

FIG. 8. Rates in various (b, a): $(20 \times 0.5, 20)$ in solid black, $(20, 20)$ in dashed red, $(20 \times 1.5, 20)$ in dotted-dashed blue, and $(20 \times 2, 20)$ in dotted black.

excellent except at special points of photon energies and emission angles.

In the following subsection we point out the relevance of the Bessel function to the Floquet system governed by a linear set of ordinary differential equations having a periodic coefficient function.

2. Floquet system

We point out the relevance of the problem to the Floquet system [10]. The function $Y(u) = \cos \Phi(u)$ along with $Z(u) = \sin \Phi(u)$ satisfies

$$\frac{d}{du} \begin{pmatrix} Y \\ Z \end{pmatrix} = \Phi'(u) \begin{pmatrix} 0 & -1 \\ 1 & 0 \end{pmatrix} \begin{pmatrix} Y \\ Z \end{pmatrix}, \qquad \text{(B7)}$$

$$\Phi'(u) = b - a \cos(u - \theta'). \qquad \text{(B8)}$$

Unlike $\Phi(u)$, its derivative $\Phi'(u)$ here is periodic. The general theorem [10] states that solutions (Y, Z) are written by

$$\cos(\mu t) \quad \text{or} \quad \sin(\mu t) \times P(t),$$

$$P(u + T) = P(u) \left(\text{periodic function of period} T = \frac{2\pi}{\beta} \rho \right).$$
$$\text{(B9)}$$

Eigenvalues $\lambda_j = i\mu_j \equiv \lambda$, $j = 1, 2$ are determined by solving differential equations in one period under the boundary conditions $(Y(0), Z(0)) = (1, 0), (0, 1)$. In terms of solutions written in the matrix form $\Psi(t)$ the eigenvalue equation is

$$\det \left(\Psi(T) - \lambda \right) = 0. \qquad \text{(B10)}$$

It is found that for large values of $b \sim a$ a large time integral may be obtained, but it depends on how close these two values are. It is important to differentiate two cases of $b \leq a$ and $b > a$ in which stationary points of $\Phi' = 0$ do or do not exist. Some cases of $b > a$ are illustrated in Fig. 8. To understand deeper, we plotted the phase function $\cos \Phi(u)$ and its integral $\int_0^u dy \cos \Phi(y)$ in Fig. 9, one case showing a steady increase over one period of circulation and the other case showing a failed increase. A nearly plateaulike region of the phase itself at a relatively early phase of circulation is a crucial condition leading to the stable phase of the rate integral.

Using the terminology of periodic potentials that one encounters in solid state physics, one would say that large rate integrals occur when parameters a, b (necessarily in the stability band due to bounded functions of sinusoidal functions) are near the boundary to the instability band. The situation may be phrased in a different way. One may introduce another function, namely, the phase integral itself,

$$W(u) = \int_0^u dy \cos \Phi(y). \qquad \text{(B11)}$$
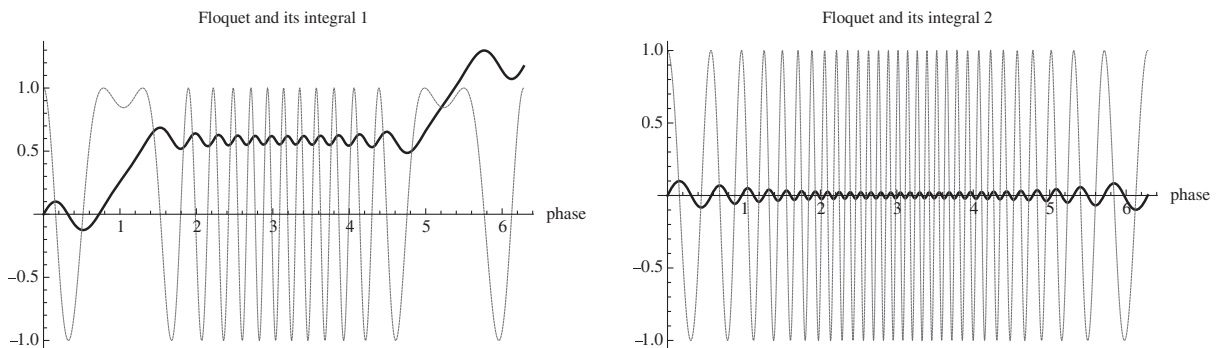

FIG. 9. $\cos \Phi(u)$ and its integral for a combination of (b, a) Left panel: $(20 \times 0.5, 20)$, with $\cos \Phi(u)$ in dotted black and its integral in solid black. Right panel: $(20 \times 0.5, 20)$.

The three-function system (X, Y, W) now satisfies a closed set of differential equations whose coefficient functions are periodic. This time the new W may not be bounded; hence this Floquet system may belong to the instability band for particular regions of (a, b). It would be useful to explore more of these features from the point of instability/stability band structure and identify quantitatively the large rate region.

---

[1] M. Yoshimura and N. Sasao, Neutrino pair and gamma beams from circulating excited ions, Phys. Rev. D **92,** 073015 (2015).

[2] J. Schwinger, On the classical radiation of accelerated electrons, Phys. Rev. **75,** 1912 (1949); The quantum correction in the radiation by energetic accelerated electrons, Proc. Natl. Acad. Sci. U.S.A. **40,** 132 (1954).

[3] A. A. Sokolov and I. M. Ternov, *Synchrotron Radiation* (Akademie-Verlag, Berlin, 1968).

[4] For a textbook description in classical electrodynamics, see J. D. Jackson, *Classical Electrodynamics* (John Wiley and Sons, Inc., New York, 2001), 3rd ed.

[5] M. Yoshimura and N. Sasao, Phys. Lett. **753,** 465 (2016).

[6] T. Asaka, M. Tanaka, and M. Yoshimura, Basic measurables in the neutrino pair beam, arXiv:1512.08076.

[7] T. Masuda, A. Yoshimi, and M. Yoshimura, A new method of creating high intensity neutron source, arXiv:1604.02818v2.

[8] C. J. Foot, *Atomic Physics* (Oxford University Press, New York, 2005).

[9] *NIST Handbook of Mathematical Functions* (Cambridge University Press, Cambridge, England).

[10] H. Hochstadt, *Differential Equations* (Dover Publication, New York, 1963), Chap. 5.